nature communications

Article

https://doi.org/10.1038/s41467-023-40415-6

Electro-assisted methane oxidation to formic acid via in-situ cathodically generated H_2O_2 under ambient conditions

Received: 16 November 2022

Accepted: 26 July 2023

Published online: 05 August 2023

Check for updates

Jiwon Kim[1,2,7], Jae Hyung Kim[3,7], Cheoulwoo Oh[1,2], Hyewon Yun[4,5], Eunchong Lee[4], Hyung-Suk Oh[2,6], Jong Hyeok Park[1] ✉ & Yun Jeong Hwang[4,5] ✉

Direct partial oxidation of methane to liquid oxygenates has been regarded as a potential route to valorize methane. However, CH_4 activation usually requires a high temperature and pressure, which lowers the feasibility of the reaction. Here, we propose an electro-assisted approach for the partial oxidation of methane, using in-situ cathodically generated reactive oxygen species, at ambient temperature and pressure. Upon using acid-treated carbon as the electrocatalyst, the electro-assisted system enables the partial oxidation of methane in an acidic electrolyte to produce oxygenated liquid products. We also demonstrate a high production rate of oxygenates (18.9 μmol h^{-1}) with selective HCOOH production. Mechanistic analysis reveals that reactive oxygen species such as •OH and •OOH radicals are produced and activate CH_4 and CH_3OH. In addition, unstable CH_3OOH generated from methane partial oxidation can be additionally reduced to CH_3OH on the cathode, and so-produced CH_3OH is further oxidized to HCOOH, allowing selective methane partial oxidation.

Methane, the main component of natural gas, has been an important resource for energy and chemical production owing to its abundance and high energy density (55 MJ kg^{-1})[1,2]. Unfortunately, the utilization of natural gas has been hampered by the difficulty of its long-distance transportation in gaseous form, and unavailable methane has been flared into CO_2, a form of less potent greenhouse gas, in oil fields (143 billion m^3 of natural gas was flared in 2020 globally)[3,4]. The methane partial oxidation to liquid oxygenates such as CH_3OH and HCOOH has been regarded as a promising approach for effective natural gas utilization as it can facilitate transportation and storage and mitigate CO_2 emission[5–7]. However, methane is a stable non-polar hydrocarbon ($\Delta H_{C\text{-}H}$ = 439.3 kJ mol^{-1}) that is challenging to activate[8]. Moreover, the complete oxidation of methane to CO_2 is more favorable than its partial oxidation (Eqs. (1, 2)). Hence, it is still challenging to induce the partial oxidation of methane without over-oxidizing it to CO_2.

$$CH_4(g) + \tfrac{1}{2}O_2(g) \rightarrow CH_3OH(l) \quad \triangle G^o = -114\ \text{kJmol}^{-1} \tag{1}$$

$$CH_4(g) + 2O_2(g) \rightarrow CO_2(g) + 2H_2O(l) \quad \triangle G^o = -804\ \text{kJmol}^{-1} \tag{2}$$

For the production of methanol or other liquid products from methane, the current industrial process relies on the following two-step indirect route: steam methane reforming (SMR) to syngas

[1]Department of Chemical and Biomolecular Engineering, Yonsei-KIST Convergence Research Institute, Yonsei University, 50 Yonsei-ro, Seodaemun-gu, Seoul 120-749, Republic of Korea. [2]Clean Energy Research Center, Korea Institute of Science and Technology, Hwarang-ro 14-gil 5, Seoul 02792, Republic of Korea. [3]Clean Fuel Research Laboratory, Korea Institute of Energy Research, Daejeon 34129, Republic of Korea. [4]Department of Chemistry, Seoul National University, Seoul 08826, Republic of Korea. [5]Center for Nanoparticle Research, Institute for Basic Science (IBS), Seoul 08826, Republic of Korea. [6]KIST-SKKU Carbon-Neutral Research Center, Sungkyunkwan University (SKKU), Suwon 16419, Republic of Korea. [7]These authors contributed equally: Jiwon Kim, Jae Hyung Kim. ✉e-mail: lutts@yonsei.ac.kr; yjhwang1@snu.ac.kr

(CO and H_2) at a high temperature (700–1000 °C) and pressure (5–40 bar) followed by a gas-to-liquid process[9]. Since SMR process has high emission of CO_2, at almost 9 kg of CO_2 per 1 kg of H_2 produced, and requires energy-intensive and large infrastructure, it is infeasible at remote geographical locations[10,11]. Therefore, energy-efficient, low CO_2 emission, and miniaturized technologies are highly required for direct partial oxidation of methane.

To date, many approaches have been developed for direct methane partial oxidation via thermocatalytic reactions; however, they need to be improved in terms of both efficiency and catalyst/oxidant candidates. Early studies employed liquid-phase homogeneous catalysis using complexes of low-valence precious metals (Hg, Pt, and Au) with a strong acid, such as oleum[12–14]. These systems, however, require highly corrosive solvents and additional hydrolysis steps for product extraction. In later studies, bioinspired Cu- or Fe-exchanged zeolite catalysts were exploited with N_2O, O_2, or H_2O oxidants for stepwise methane conversion in the gas phase[15–17]. Although high selectivity was achieved, such conversions suffer from low reaction rates, high reaction temperature (300–550 °C), and catalyst regeneration step. Recently, an aqueous-phase partial oxidation of methane over Fe and Rh catalysts using H_2O_2 as the oxidant was reported[18–20]. Although higher production yield and selectivity were achieved, the high cost of H_2O_2, which is more expensive than the reaction products, limits the practical application of this process. Therefore, efforts have been made to convert methane to oxygenates using in-situ H_2O_2[5,21,22] generated from O_2 and H_2 over a catalyst such as AuPd or PdCu[5,21]. However, such conversions require H_2 as a co-reductant, precious metal catalysts, and elevated temperatures (70–120 °C). Hutchings et al. reported an Au-ZSM-5 catalyst using O_2 as the sole oxidant for the partial oxidation of methane; however, the reaction conditions were still harsh (120–240 °C and 23.2 bar)[22]. For conducting partial oxidation of methane in industrial areas, systems with mild reaction conditions should be developed using earth-abundant materials and eco-friendly oxidants.

While thermocatalytic oxidation reactions often require a high temperature and pressure, electrochemical oxidation can be conducted under ambient conditions. It offers a sustainable route for converting CH_4 to liquid fuels, mitigating CO_2 emissions[23–29]. For electrochemical methane oxidation, the formation of active oxygen species (e.g., O^{2-} and O^-) on the electrocatalysts is necessary. Bertazzoli et al. succeeded in producing CH_3OH, HCHO, and HCOOH as liquid products from methane using TiO_2/RuO_2 and $V_2O_5/TiO_2/RuO_2$ electrocatalysts[23,24]. NiO/Ni catalyst has also been reported to generate C_2H_5OH, and CH_3OH in an H-cell[26]. However, the production rates of oxygenates were insufficient possibly due to the over-oxidation of the products to CO_2 or the competitive oxygen evolution reaction. To resolve these issues at the anode, electro-assisted methane partial oxidation (EMPO) at the cathode side has been proposed[27–29]. By reacting methane with the active oxygen species generated from the electrochemical oxygen reduction reaction (ORR), methane partial oxidation could be accomplished. However, there are only few reports about EMPO systems, and the reaction mechanism of EMPO is unclear.

In this study, we systematically investigate the EMPO system and demonstrate its promising production rate of oxygenates for methane partial oxidation. The EMPO system involves both electrochemical and chemical reactions. In this system, H_2O_2 is electrochemically produced on the cathode through a two-electron pathway ORR, and the H_2O_2 production involves oxidizing methane in the catholyte. The EMPO process can provide a high oxygenates production rate of 18.9 μmol h^{-1} at room temperature and atmospheric pressure. Mechanistic investigations indicate that the EMPO system is beneficial for selective methane oxidation to HCOOH. Reactive oxygen species (ROSs) (i.e., •OH and •OOH radicals) are generated during ORR and activated CH_4 and CH_3OH. CH_3OOH is one of the major products in methane partial oxidation; however, it is not a suitable liquid fuel for long-distance transportation because of its instability. In the EMPO system, most of the produced CH_3OOH is electrochemically reduced to CH_3OH on the cathode, and CH_3OH is further oxidized to HCOOH, resulting in high selectivity to HCOOH (80.7%). We also demonstrate that the electro-assisted oxidation process can be a general approach for the partial oxidation of small hydrocarbons such as ethane. We envisage that this miniaturized and sustainable system can provide a beneficial strategy for direct methane partial oxidation.

Results

Feasibility study of EMPO system

First, an acid-treated ketjen black (a-KB) carbon powder catalyst was prepared as a selective cathode catalyst for generating H_2O_2 via the two-electron pathway ORR[30,31]. Pristine ketjen black (KB) powder was acid-treated at an elevated temperature (80 °C) to introduce oxygen functional groups (−COOH and C−O−C), which are active in two-electron ORR. X-ray photoelectron spectroscopy (XPS) was performed to examine the changes in oxygenated species on the surface of the acid-treated carbon powder. (Supplementary Fig. 1). The C 1*s* spectrum of a-KB could be deconvoluted into bands attributed to the following species: graphitic carbon (C−C) at 284.8 eV, defects attributed to amorphous carbon at 285.9 eV, carbon singly bound to oxygen (C−O) at 286.8 eV, carbon bound to two oxygen atoms (i.e., −COOH) at 288.8 eV, and carbon in an aromatic ring at 291.2 eV ($\pi-\pi^*$ transitions)[32,33]. Deconvolution of the O 1*s* peak resulted in two peaks: oxygen doubly bound to carbon (C=O) at 533.7 eV and oxygen singly bound to carbon (C−O) at 532.1 eV[34]. Both the C 1*s* and O 1*s* signals indicate an increase in oxygenated species with C−O and C=O functional groups (e.g., C−OH, C−O−C, and O=C−OH) after acid treatment. High-resolution transmission electron microscopy (HR-TEM) and energy-dispersive X-ray spectroscopy (EDS) mapping images of a-KB revealed that the oxygen functional groups were well distributed over the surface of carbon (Supplementary Fig. 2). The ORR performance of a-KB was then evaluated in an aqueous solution (0.05 M H_2SO_4) using the rotating ring-disk electrode (RRDE) technique. The polarization curves of the catalyst (Supplementary Fig. 3) indicate that the onset potential is ~0.3 V (vs. reversible hydrogen electrode (RHE)). Furthermore, the a-KB catalyst exhibited a high H_2O_2 selectivity of >90% over the applied potential ranges (0–0.3 V vs. RHE).

Next, to demonstrate the proposed EMPO system mediated by in-situ cathodic H_2O_2 generation, we conducted the reaction in an H-type cell (Fig. 1a). The working electrode was prepared by spraying a-KB based catalyst ink on carbon paper. The EMPO was carried out in a 0.05 M H_2SO_4 electrolyte with continuous feeding of O_2 and CH_4 gases. The potential was maintained at 0 V (vs. RHE), at which H_2O_2 was selectively produced from ORR (Supplementary Fig. 3), and the reaction was conducted at 25 °C for 30 min. ^1H and ^{13}C nuclear magnetic resonance (NMR) spectra were obtained to analyze the liquid products using an internal standard. Figure 1b shows that CH_3OH, CH_3OOH, and HCOOH were generated as liquid products of the partial oxidation of methane. No liquid products were detected when Ar was fed instead of CH_4[18,35]. The isotope experiment using $^{13}CH_4$ corroborated that $H^{13}COOH$ originated from the methane partial oxidation, as shown in Fig. 1c and Supplementary Fig. 4 (CH_3OH and CH_3OOH could not be detected because of the sampling method)[36]. We conducted an EMPO reaction applying Au foil as a carbon-free ORR catalyst, and the HCOOH was also generated as a liquid product confirming that the reaction products are generated from CH_4 oxidation (Supplementary Fig. 5). Then we analyzed time-dependent product formation under 0 V (vs. RHE), which further verified that the amount of the major product, HCOOH, increased linearly with the reaction time (Fig. 1d), supporting the continuous EMPO process. The amounts of minor products, CH_3OOH and CH_3OH, increased to a certain level and remained constant. The different behaviors of time-dependent products' amounts originate from the reaction mechanism of EMPO,

https://doi.org/10.1038/s41467-023-40415-6

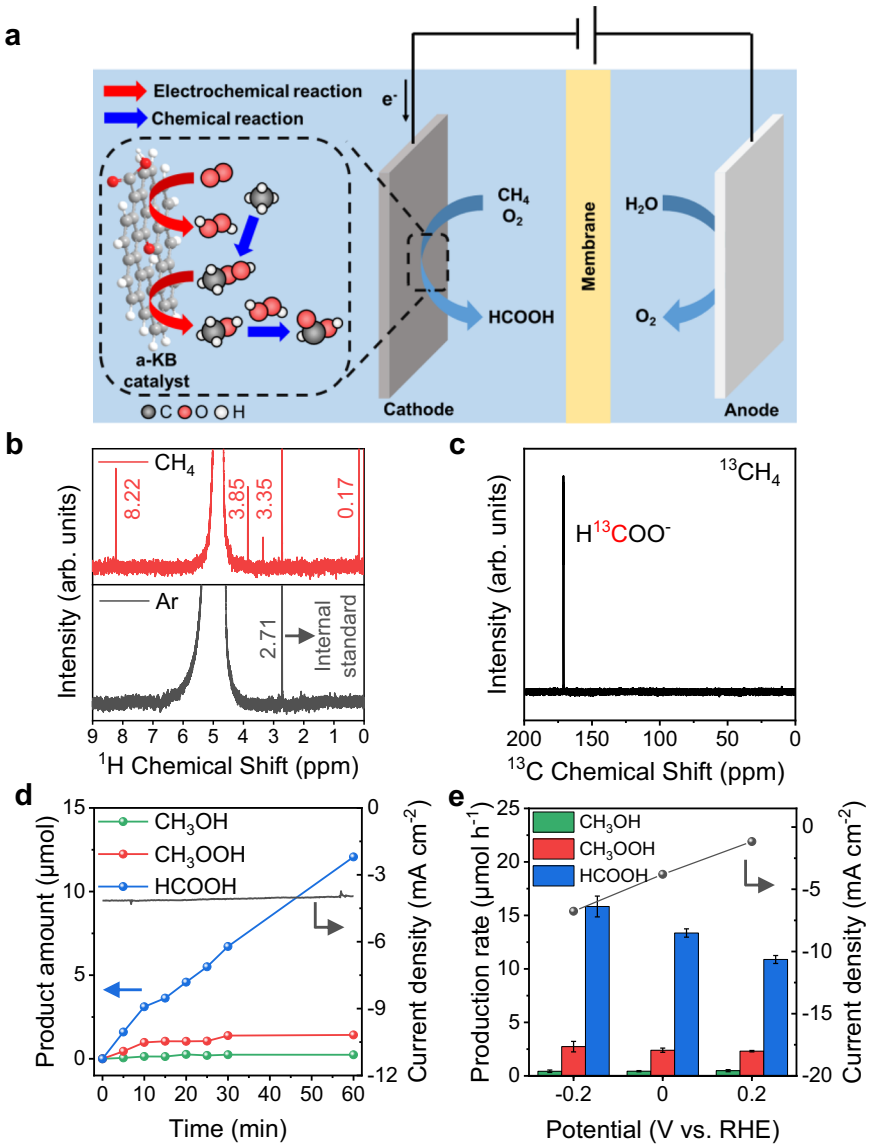

Fig. 1 | Electro-assisted selective CH_4 partial oxidation system. a Schematic illustration of the EMPO system. **b** ^{1}H-NMR spectra of the products after reaction with purging CH_4 (red) or Ar (gray) along with O_2. The peaks at 0.17, 2.71, 3.35, 3.85, and 8.22 ppm are attributed to CH_4, $(CH_3)_2SO$ (DMSO), CH_3OH, CH_3OOH, and HCOOH, respectively. **c** ^{13}C-NMR spectrum of the product after EMPO using $^{13}CH_4$. The peak at 166 ppm is attributed to $H^{13}COO^-$. **d** Time-dependent change in the amounts of liquid products of EMPO. **e** Potential-dependent production rates of liquid products of EMPO. Reaction conditions: 25 °C, 1 bar, 30 min, O_2: 100 sccm, CH_4: 100 sccm, 55 mL of 0.05 M H_2SO_4, and stirring at 700 rpm. The error bars represent the standard deviation. Source data are provided as a Source Data file.

which is later discussed. Additionally, we investigated whether gas products such as CO and CO_2 were generated due to the over-oxidation of CH_4 by on-line gas chromatography (GC). During the EMPO reaction, the amount of the produced CO_2 was 0.76 μmol h^{-1} which was an insignificant amount compared to that of HCOOH (13.8 μmol h^{-1}) (Supplementary Figs. 6, 7).

Then other parameters, which can affect production rates, such as flow rate and applied potential were examined. First, we increased the flow rates of both feeding gases (CH_4 and O_2) from 100 sccm to 200 sccm (Supplementary Fig. 8a). The same product amounts were observed meaning that these total flow rates do not have an impact on the EMPO reaction rate (i.e., sufficient supply of reactant gases). On the other hand, the production of HCOOH is influenced by changes in the partial concentrations of CH_4 and O_2 (Supplementary Fig. 8b). To control the CH_4:O_2 ratio, we reduced the CH_4 flow rate to 25 sccm while maintaining the O_2 flow rate (resulting in a decrease in the partial pressure of CH_4), which led to a decrease in the amount of HCOOH produced. In contrast, when the flow rate of O_2 was reduced to 25 sccm while keeping the CH_4 flow rate constant, the production of HCOOH increased. As the flow rate of CH_4/O_2 changed from 25 sccm/100 sccm to 50 sccm/50 sccm to 100 sccm/25 sccm, the partial concentration of CH_4 increased from 20% to 50% to 80%. The amount of HCOOH produced increased in the order of increasing partial concentration of CH_4, indicating that CH_4 was the limiting reagent and affected the reaction rate under these EMPO conditions.

In addition, the production rate depended on the applied potential (Fig. 1e) and is related to the amount of cathodically generated H_2O_2. As the applied potential was swept from +0.2 to −0.2 V (vs. RHE) (i.e., as the cathodic current increased), the amounts of oxygenated liquid products increased due to increased H_2O_2 generation. The highest production rate of the total oxygenates was 18.9 μmol h^{-1} (CH_3OH: 0.4 μmol h^{-1}, CH_3OOH: 2.7 μmol h^{-1}, and HCOOH: 15.8 μmol h^{-1}). Although the production rate increased at −0.2 V (vs. RHE), the hydrogen evolution reaction can occur competitively below 0 V (vs. RHE) in an acidic electrolyte. Therefore, we performed the subsequent experiments at 0 V (vs. RHE).

https://doi.org/10.1038/s41467-023-40415-6

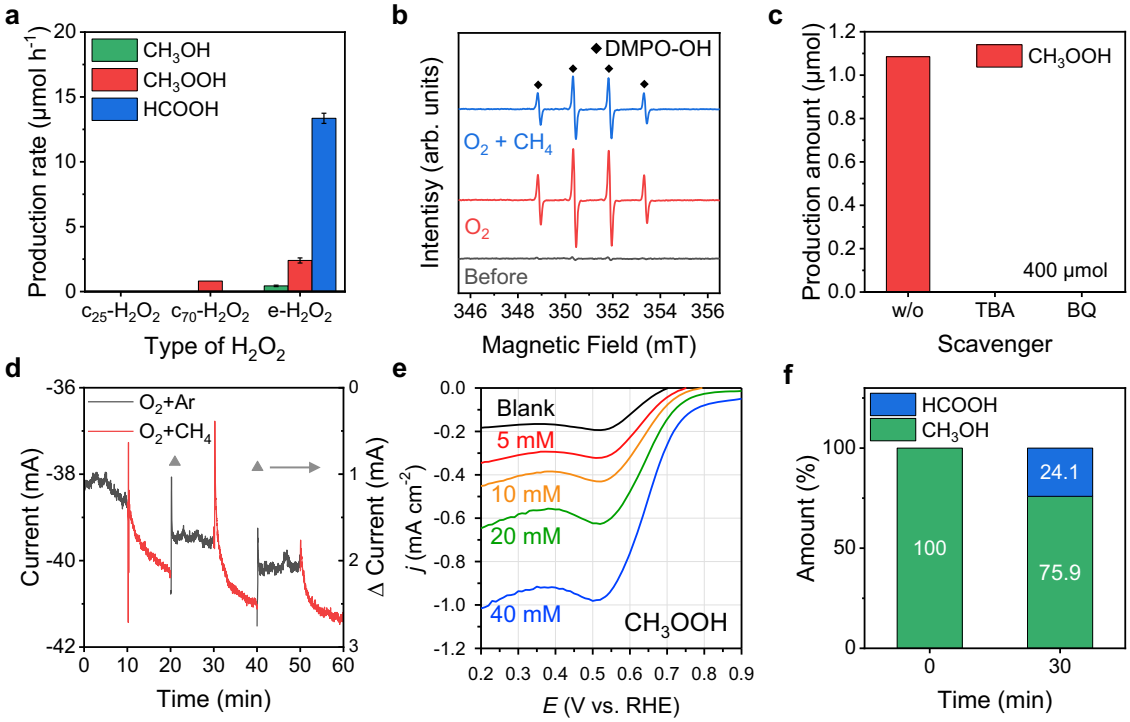

Fig. 2 | Electrochemical analysis of EMPO. a Performance comparison of a system using commercial H_2O_2 (c_{25}-H_2O_2 and c_{70}-H_2O_2 indicate reactions conducted at 25 °C and 70 °C, respectively) and the EMPO system (e-H_2O_2). The error bars represent the standard deviation. **b** EPR spectra of the electrolytes before (gray line) and after applying potential (0 V vs. RHE) under O_2(g) (red line) and O_2(g)+CH_4(g) (blue line) flowing with DMPO. **c** CH_3OOH production after EMPO reaction in the presence of 400 μmol of scavengers. TBA and BQ are radical scavengers that can trap •OH and •OOH, respectively. **d** Chronoamperometry under O_2 + Ar and O_2 + CH_4 purging at 0 V (vs. RHE); O_2, Ar, and CH_4: 100 sccm. **e** Polarization curves in the presence of 0–40 mM of CH_3OOH in a 0.05 M H_2SO_4 electrolyte. The black, red, orange, green, and blue lines represent blank, 5, 10, 20, and 40 mM conditions, respectively. **f** Result of methanol oxidation using ORR. Source data are provided as a Source Data file.

Investigation of the reaction mechanism of EMPO

Next, we explored the reaction mechanism of EMPO mediated by in-situ generated H_2O_2. First, we compared the performances of the EMPO system (e-H_2O_2) and a non-electro-assisted system using commercial H_2O_2 (c-H_2O_2) as the oxidant (Fig. 2a). In the c-H_2O_2 system, c-H_2O_2 was supplied with a syringe pump, and the injection rate was controlled to be the same as the H_2O_2 production rate estimated from the $2e^-$ ORR activity in our EMPO system (calculated based on the RRDE analysis). Other reaction conditions such as the electrolyte (0.05 M H_2SO_4) and reaction time (30 min) were the same, except for the feeding of O_2 gas. In contrast with EMPO, no liquid products were formed when c-H_2O_2 was added to the reaction cell at 25 °C (Fig. 2a and Supplementary Figs. 9, 10) implying that H_2O_2 molecule itself cannot react with CH_4 and ROSs formed during electrochemical ORR are crucial for the EMPO[37,38].

We performed control experiments to figure out whether ROSs are generated from O_2 and participate in the EMPO reaction. To understand the role of O_2 in the EMPO reaction, we applied the same cathodic potential in the H-cell under CH_4 and Ar flow. No CH_4 oxidation products were detected after the reaction feeding CH_4 + Ar except O_2 (Supplementary Fig. 11), supporting that O atoms from O_2(g) not from the H_2O electrolyte participate in activating CH_4. Then, to verify radical species more directly, we additionally conducted electron paramagnetic resonance (EPR) analysis by adding 5,5-dimethyl-1-pyrroline N-oxide (DMPO) in the electrolytes as a spin trap. EPR signals were collected by measuring electrolytes before and after applying reduction potential (0 V vs. RHE) flowing O_2(g) or O_2(g)+CH_4(g) under the addition of DMPO (Fig. 2b). We confirmed that no radical signal was observed in the electrolyte before the reaction (gray line). Meanwhile, a quartet spectrum with a relative intensity ratio of 1:2:2:1 appeared after applying potential under O_2 + CH_4 feeding (blue line). It is typically attributed to the formation of DMPO–OH adducts supporting that radicals were formed during the EMPO reaction[39]. Especially, DMPO–OH adducts were also detected when only O_2 was fed without CH_4 suggesting that ROSs are generated as the result of electrochemical ORR in our system (red line). Although the signal corresponding to DMPO–OH adducts was the only EPR signal detected, the formation of other ROSs cannot be excluded because other DMPO–ROS adducts have a short lifetime and quickly decompose to the DMPO–OH adduct[40]. Therefore, we further performed trapping experiments applying tert-butyl alcohol (TBA) and 1,4-benzoquinone (BQ) as •OH and •OOH radical scavengers, respectively. To identify the effects of the ROSs, we measured the product amount of CH_3OOH in the presence or absence of the radical scavengers. No CH_3OOH was detected under an excess amount (400 μmol) of scavengers (Fig. 2c). When 40 μmol of TBA and BQ were present in the electrolytes, respectively, the generated amount of CH_3OOH was decreased compared to the case without these scavengers (Supplementary Fig. 12). These series results indicate that ROSs generated from O_2 activate CH_4 to produce CH_3OOH.

Then, the reaction temperature was increased to 70 °C to activate c-H_2O_2. At 70 °C, the c-H_2O_2 reacted with CH_4, but only unstable CH_3OOH was produced at 0.8 μmol h^{-1} production rate (Fig. 2a and Supplementary Fig. 13), which was much lower production than that of the EMPO system at room temperature. Other reaction temperatures (50–90 °C) were also tested using c-H_2O_2 and all showed only a small amount of CH_3OOH production (Supplementary Figs. 13, 14). The production rate of the unstable CH_3OOH rather decreased as the reaction temperature increased from 70 °C to 90 °C. This supports that the electro-assisted system (e-H_2O_2) contributes to the increase in liquid products. Based on these results, we speculated that the EMPO system not only guides the reaction between CH_4 and

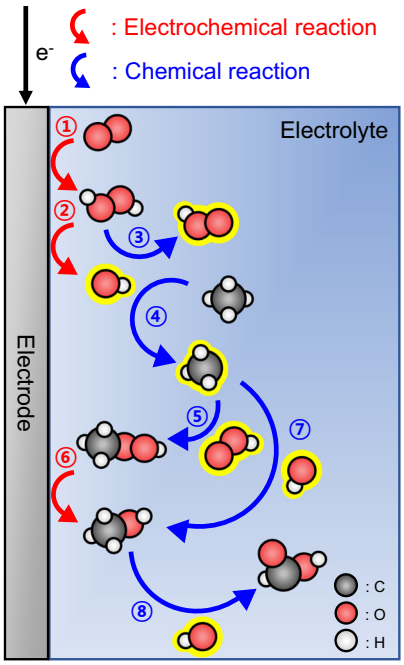

ROSs formation:
$O_2 + 2H^+ + 2e^- \rightarrow H_2O_2$ ①
$H_2O_2 + e^- \rightarrow \cdot OH + OH^-$ ②
$\cdot OH + H_2O_2 \rightarrow \cdot OOH + H_2O$ ③

CH_4 activation:
$CH_4 + \cdot OH \rightarrow CH_3\cdot + H_2O$ ④

CH_3OOH formation:
$CH_3\cdot + \cdot OOH \rightarrow CH_3OOH$ ⑤

CH_3OH formation:
$CH_3OOH + 2H^+ + 2e^- \rightarrow CH_3OH$ ⑥
$CH_3\cdot + \cdot OH \rightarrow CH_3OH$ ⑦

HCOOH formation:
$CH_3OH + 4\cdot OH \rightarrow HCOOH + 3H_2O$ ⑧

Fig. 3 | Proposed reaction mechanism of EMPO. Schematic illustration of the reaction mechanism for selective HCOOH production by EMPO. The red (①,②,⑥) and blue (③,④,⑤,⑦,⑧) arrows and numbers represent electrochemical and chemical reactions, respectively. The black, red, and white balls represent C, O, and H atoms, respectively.

electrochemically generated H_2O_2 but also alters the selectivity of the reaction and enhances the production rate.

$$CH_3OOH + 2H^+ + 2e^- \rightarrow CH_3OH + H_2O \quad E^o = 1.70\text{V vs. RHE} \qquad (3)$$

Considering the standard reduction potential of CH_3OOH (Eq. (3)), it can be easily reduced to CH_3OH at the working potential of the EMPO system. We investigated the additional reduction of CH_3OOH on the electrode through control experiments. We conducted chronoamperometry at 0 V (vs. RHE) with alternating supply of O_2 + Ar and O_2 + CH_4 gas mixtures for 10 min each (Fig. 2d) to understand whether the supply of CH_4 affects the current density of the reaction. While the ORR can occur under O_2 + Ar conditions, under O_2 + CH_4 conditions, the generation of oxygenates and their sequential reduction can occur together with the ORR. The current during the O_2 + CH_4 supply was always higher than that during the O_2 + Ar supply, and the cathodic current density increased slowly, implying that CH_4 induced additional reduction reactions. To determine whether oxygenated products were electrochemically reduced further on the cathode, we performed linear sweep voltammetry to study the reduction capabilities of CH_3OOH, CH_3OH, and HCOOH at the EMPO working potential using various concentrations (0–40 mM) of these compounds[41,42]. As shown in Fig. 2e, the reduction current increased with increasing CH_3OOH concentration, indicating its easy reducibility. In contrast, the polarization curves of the systems containing CH_3OH and HCOOH exhibited no significant differences with the increase in their concentrations (Supplementary Fig. 15). These results suggest that CH_3OH and HCOOH cannot be reduced on the a-KB cathode under these conditions, and the current increase observed in Fig. 2d is due to the reduction of CH_3OOH.

In addition, to confirm whether CH_3OH can be oxidized to HCOOH in the presence of ROSs, we conducted CH_3OH oxidation experiments using c-H_2O_2 and e-H_2O_2 at room temperature. Similar to CH_4, CH_3OH was oxidized to HCOOH only by in-situ generated H_2O_2 (e-H_2O_2) and no CH_3OOH was produced (Supplementary Figs. 16, 17 and Fig. 2f)[18,35,43,44]. We also investigated the EMPO reaction under the alkaline electrolyte (0.1 M KOH). Although an a-KB exhibited high selectivity to H_2O_2 from ORR in the alkaline condition, no products from CH_4 oxidation were observed. This implies that the coupling between ORR and CH_4 oxidation reaction is influenced by the pH of the electrolyte, favoring the acidic condition for the EMPO reaction (Supplementary Figs. 18, 19).

Proposed mechanism

Based on the above electrochemical analyses, we deduced the reaction mechanism of EMPO. As illustrated in Fig. 3, first, O_2 is reduced to H_2O_2 on the electrode through the electrochemical two-electron pathway ORR, and ROSs are formed (ROSs formation). Second, •OH radicals activate CH_4 to produce CH_3• radicals in the electrolyte (CH_4 activation). Then, CH_3OOH is generated by the reaction between CH_3• and •OOH radicals (CH_3OOH formation). Subsequently, CH_3OH was generated by electrochemical reduction of CH_3OOH and radical reaction between CH_3• and •OH. Finally, HCOOH was formed in the presence of •OH radicals (HCOOH formation). Thus, HCOOH can be generated as a selective reaction product with the aid of electrochemical reduction potential at room temperature and atmospheric pressure in the EMPO system.

Electro-assisted C_2H_6 partial oxidation

To validate the electro-assisted C−H activation of alkane for partial oxidation products generation, the C_2H_6 partial oxidation was examined under the same cathodic H_2O_2 generation conditions. All the reaction conditions were maintained the same, except that C_2H_6 was used instead of CH_4. In this case, C_2 oxygenates (C_2H_5OH, C_2H_5OOH, and CH_3COOH) and C_1 oxygenates (CH_3OH, CH_3OOH, and HCOOH) were obtained as the products (Supplementary Fig. 20). The exclusive observation of the C_2 partial oxidation products are supporting direct C−H activation from C_2H_6. The reaction products were changed from C_1 (CH_3OH, CH_3OOH, and HCOOH) to C_2 (C_2H_5OH, C_2H_5OOH, and CH_3COOH) with similar oxidation states by simply replacing CH_4(g) with C_2H_6(g) under the same reaction conditions. The reaction pathway is similar to that of EMPO. As C_2H_6 is more reactive ($\Delta H_{C\text{-}H} = 421.7$ kJ mol^{-1})[45,46] than methane, the activation of C_2H_6 via C−H bond breakage can occur more easily, resulting in

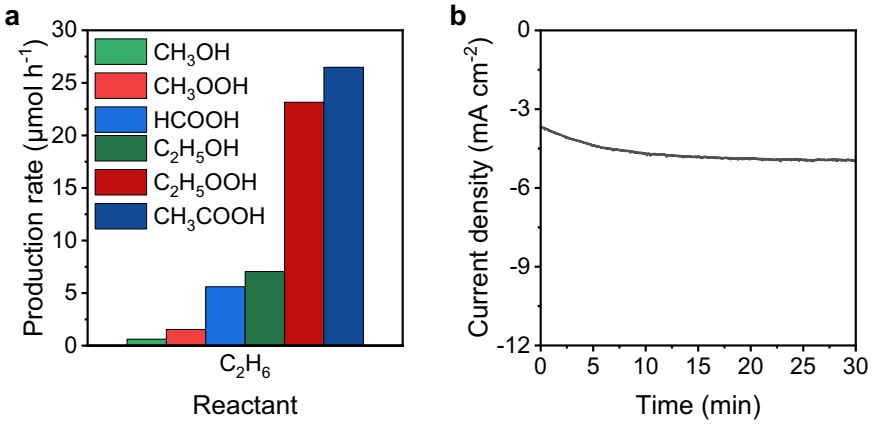

Fig. 4 | Electro-assisted C_2H_6 partial oxidation. a Production rate of electro-assisted ethane partial oxidation. **b** Current density during the reaction time. Reaction conditions: 25 °C, 1 bar, 30 min, O_2: 100 sccm, C_2H_6: 100 sccm, 55 mL of 0.05 M H_2SO_4, stirring at 700 rpm, and 0 V (vs. RHE). Source data are provided as a Source Data file.

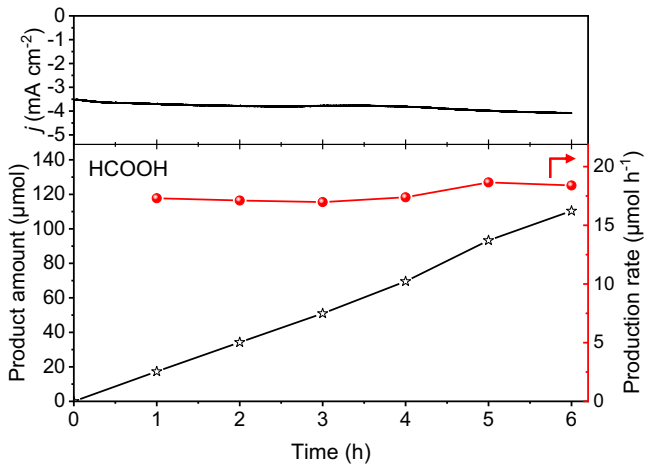

Fig. 5 | Stability test of the EMPO system. EMPO reaction during 6 h. Reaction conditions: 25 °C, 1 bar, O_2: 100 sccm, CH_4: 100 sccm, 550 mL of 0.05 M H_2SO_4 circulated by 10 mL min^{-1}, stirred at 700 rpm, and 0 V (vs. RHE). Source data are provided as a Source Data file.

higher total product yield than that of the EMPO system (Figs. 4a, 2a). Further, C − C bond breakage can lead to C_1 oxygenates products. The increased current compared with that of EMPO (Fig. 2a) is attributed to the relatively high concentration of reaction intermediates that can be reduced on the electrode. Through the electro-assisted C_2H_6 partial oxidation, we confirmed that electrochemically generated H_2O_2 can also activate C_2H_6, leading to the production of partially oxidized products. This reaction also demonstrates the general applicability of the electro-assisted system in the partial oxidation of saturated hydrocarbons. Thus, the EMPO system can be adopted as a general partial oxidation system for small hydrocarbons.

Stability test

A stability test of the EMPO system was performed (Fig. 5). The stability test was conducted under the electrolyte-flowing H-cell setup to keep HCOOH concentration low because the high concentration of HCOOH induces over-oxidation to CO_2 (Supplementary Figs. 21, 22). During six hours of the EMPO reaction, no decreases in the current density or production rate of HCOOH were observed demonstrating its stable operation. It is attributed to the stability of metal-free carbon catalyst which operates stably under acidic condition. Additionally, it was confirmed that no Pt metal impurities were detected in either the catalyst or solution after the reaction by inductively coupled plasma optical emission spectroscopy (ICP-OES) (Supplementary Table 1). The HCOOH production rate in our EMPO process was kept high, and the reaction proceeded under ambient pressure and temperature (Supplementary Fig. 23 and Supplementary Table 2)[7,22,47–54].

Discussion

In this study, we investigated an EMPO system for the partial oxidation of methane at room temperature and ambient pressure with the assistance of electrochemically in-situ generated H_2O_2 on the cathode. The EMPO process involves cathodic H_2O_2 production from the ORR and subsequent partial oxidation of methane, resulting in selective HCOOH production in the acidic condition. Metal-free a-KB was utilized as the catalyst to generate H_2O_2 via the two-electron pathway ORR. CH_3OH, CH_3OOH, and HCOOH were obtained as liquid products of EMPO reaction with a total oxygenate production rate of 18.9 μmol h^{-1} under ambient pressure and temperature. Through a mechanistic study of the EMPO process, we propose that ROSs are the active species of the partial oxidation of CH_4. CH_4 can be activated by the in-situ cathodically generated ROSs (i.e., •OH and •OOH radicals) from the O_2 reduction. Additionally, the unstable CH_3OOH product can be converted to CH_3OH on the cathode at the EMPO working potential; this improved product selectivity (80.7%) toward the stable liquid fuel, HCOOH. This EMPO system applying metal-free carbon catalyst showed significant stable performance for 6 h. We also demonstrated the general applicability of the electro-assisted oxidation process by activating the C−H bond of C_2H_6. In this case, various C_2 and C_1 oxygenates were produced, with C_2H_5OOH and CH_3COOH as the major products. We believe that the EMPO system is a promising route for developing a sustainable and miniaturized strategy for on-site natural gas conversion.

Methods

Acid treated ketjen black (a-KB) preparation

Ketjen black (EC-600JD) (KB) powder (1 g) was added to 250 mL of 60% HNO_3 (Samchun Chemicals) then the mixture was stirred at 80 °C in an oil bath for 12 h. After acid-treatment, acid treated ketjen black (a-KB) was vacuum-filtered and washed with copious amount of deionized (DI) water and dried in vacuum oven overnight. Finally, 800 mg of a-KB powder was obtained.

Characterization

The XPS spectra were acquired using a Nexsa (ThermoFisher Scientific) instrument with a Microfocus monochromatic Al-Kα X-ray source.

The HR-TEM was performed on a JEM-F200 (JEOL) electron microscope with 200 kV acceleration voltage. EDS mapping were analyzed by JEOL Dual SDD system with 200 kV. The ICP-OES was measured by iCAP 7000 (Thermo Scientific) to analyze the presence of Pt metal impurities in the catalyst and electrolytes.

Electrochemical ORR test

The electrochemical ORR test was performed using an electrochemical workstation (CHI760E, CH Instruments) at room temperature (25 °C) under atmospheric pressure. For the rotating ring disk electrode (RRDE) measurements, a three-electrode system was constructed with an RRDE (Pine research, E7R9 RRDE) (glassy carbon (GC) disk (0.2475 cm^2) + Pt ring (0.1866 cm^2)), a Ag/AgCl (stored in 3 M KCl, BASi) reference electrode, and a Pt foil counter electrode. The catalyst ink were prepared by dispersing the a-KB powder in solution (Ethanol (C_2H_5OH, Sigma-Aldrich, 99.5%):DI = 3.5:1) with 5 wt% Nafion (Sigma-Aldrich) to achieve concentration of ~0.01 mg μl^{-1}. After sonication for 30 min, 8 µl of the catalyst ink was drop casted onto a disk electrode and dried at room temperature. Cyclic voltammetry (CV) was performed between 0.05 and 1.20 V (vs. RHE) in N_2 (99.999%)-saturated 0.05 M H_2SO_4 (Sigma-Aldrich, 99.999%) and 0.1 M KOH (Sigma-Aldrich, 90%) at a scan rate of 100 mV s^{-1} for 10 cycles, in which steady CV response was obtained. O_2 (99.999%) gas was supplied into the electrolyte for 5 min. The impedance spectroscopy was conducted at 0.68 V (vs. RHE) from 100,000 to 1 Hz to determine the uncompensated resistance (R_u) in a high-frequency range for *iR*-correction. The H_2O_2 production activity was assessed by linear sweep voltammetry (LSV) from 1.1 to 0.2 V (vs. RHE) in O_2-saturated 0.05 M H_2SO_4 and 0.1 M KOH at a scan rate of 5 mV s^{-1} and rotating speed of 1600 rpm. During the LSV, the Pt ring potential was held at 1.23 V (vs. RHE). The H_2O_2 selectivity was calculated using the following relation:

$$H_2O_2\ \text{Selectivity}\,(\%) = 200 \times \frac{i_r/N}{i_d + i_r/N} \tag{4}$$

where i_r, N, and i_d denote the ring current, collection efficiency (37%), and disk current, respectively.

The Faradaic efficiency of H_2O_2 was calculated by equation below:

$$F.E._{\cdot H_2O_2}(\%) = 100 \times \frac{i_r/N}{i_d} \tag{5}$$

The collection efficiency (N) was determined using the $[Fe(CN)_6]^{3-/4-}$ redox system. Chronoamperometry was carried out at −0.3 V (vs. Ag/AgCl) while the ring potential was fixed at 0.5 V (vs. Ag/AgCl) for 60 s on the catalyst-deposited RRDE in N_2-saturated 0.1 M KOH + 2 mM $K_3[Fe(CN)_6]$ (Sigma-Aldrich, ≥99.0%). The background current was obtained similarly, but the disk potential was 0.5 V (vs. Ag/AgCl). The collection efficiency was calculated as follows:

$$N = \frac{|i_r - i_{r,bg}|}{i_d} \tag{6}$$

Where i_r, $i_{r,bg}$, and i_d denote the ring current, background ring current, and disk current, respectively. The collection efficiency was 37% (Supplementary Fig. 24).

Working electrode preparation

5 mg of a-KB catalyst was mixed with 1 mL of 2-propanol (IPA, Sigma Aldrich, 99.5%) and 50 µL of 5 wt% Nafion. Then the mixture was sonicated for 10 min. The catalyst ink was sprayed on the carbon paper (TGP-H-120 20%WP, Toray) (11.25 cm^2). The mass loading of a-KB on the carbon paper was 1 mg cm^{-2}.

EMPO experiment

The EMPO experiment was conducted in an H-type cell separated by Nafion 117 membrane using a potentiostat (Ivium Vertex, Ivium Technologies). A three-electrode system consisting of an a-KB sprayed carbon paper as the working electrode, Ag/AgCl (stored in 3 M KCl) reference electrode, and a Pt plate as a counter electrode was constructed. The working electrode was used without pre-activation process. The 0.05 M H_2SO_4 was used as an electrolyte (55 mL for both catholyte and anolyte). Catholyte was purged with O_2 and CH_4 (99.999%) gases for at least 30 min prior to reaction and constantly purged at a flow rate of 100 sccm during the reaction (0 V vs. RHE). The catholyte was continuously stirred at 700 rpm. Reaction temperature was maintained at 25 °C by water bath.

For the control experiment, all reaction conditions were the same except for feeding Ar gas (99.999%) instead of CH_4.

For the $^{13}CH_4$ (Icon Isotopes, 99.8%) isotope experiment, all reaction conditions were the same except for feeding $^{13}CH_4$ instead of $^{12}CH_4$.

For the carbon-free ORR catalyst experiment, Au foil (Dasom RMS, 99.99%, 11.25 cm^2) was applied for working electrode while all other reaction conditions were the same. The Au foil was used without pre-activation process.

For the time dependent production rate analysis, potential (0 V vs. RHE) was applied for 1 h and 500 µL of electrolyte was extracted for each 5, 10, 15, 20, 25, 30, and 60 min. Other reaction conditions were the same.

For the flow rate experiments, the flow rates of CH_4 and O_2 were varied from 25 sccm to 200 sccm while all other reaction conditions were maintained.

For the potential dependent production rate analysis, applied potential was varied from −0.2 to +0.2 V (vs. RHE) for 30 min. Other reaction conditions were the same.

For the identification of O source experiment, Ar was purged instead of O_2. Other reaction conditions were the same.

For the EPR experiment, 1 mmol of DMPO (Sigma-Aldrich, ≥98%) was applied as a spin trap before the reaction. Other reaction conditions were the same except for feeding O_2 or $O_2 + CH_4$ gases.

For the trapping experiments, 400 and 40 µmol of TBA (Sigma-Aldrich, ≥99.5%) and BQ (Sigma-Aldrich, ≥98%) were added before the reaction as •OH and •OOH radical scavengers, respectively. Other reaction conditions were the same.

For the chronoamperometry experiment, O_2 + Ar and $O_2 + CH_4$ (100 sccm each) were purged alternatively every 10 min for 1 h. Other reaction conditions were the same.

For the CH_3OH (Sigma-Aldrich, ≥99.9%) oxidation experiment, all reaction conditions were the same except for injecting 100 µmol of CH_3OH before the reaction instead of CH_4.

For the alkaline EMPO experiment, all reaction conditions were the same except for applying 0.1 M KOH as an electrolyte instead of 0.05 M H_2SO_4.

For the electro-assisted C_2H_6 partial oxidation experiment, all reaction conditions were the same except feeding C_2H_6 instead of CH_4.

For the stability test, the electrolyte-flowing H-cell setup was established. 550 mL of 0.05 M H_2SO_4 was circulated by 10 mL min^{-1}. The EMPO reaction was performed for 6 h. Other reaction conditions were the same.

Methane partial oxidation using commercial H_2O_2

CH_4 partial oxidation using commercial H_2O_2 (30 wt% in H_2O, Sigma-Aldrich) was conducted using cathode part of H-type cell. 55 mL of 0.05 M H_2SO_4 was filled in cathode part and the solution was purged with Ar and CH_4 at 100 sccm simultaneously. Ar was purged instead of O_2 to keep balance of partial flow of CH_4. Commercial H_2O_2 was injected during reaction time (30 min) via syringe pump. The amount

of H_2O_2 supplied was determined based on RRDE analysis.

$$The\ amount\ of\ H_2O_2 = \frac{F.E._{H_2O_2} \times j \times A \times t}{n \times F} \quad (7)$$

where, $F.E._{H2O2} = 81.8\%$, j is current density, A is area of electrode, t is reaction time, n is moles of electron to produce 1 mole of H_2O_2, and F is faraday constant. The solution was stirred at 700 rpm and kept at 25, 50, 70, or 90 °C by water bath.

Methanol oxidation using commercial H_2O_2

CH_3OH oxidation using commercial H_2O_2 was conducted using cathode part of H-type cell. 55 mL of 0.05 M H_2SO_4 was filled in cathode part and 100 μmol of CH_3OH was injected before the reaction. Commercial H_2O_2 was fed during reaction time (30 min) via syringe pump. The amount of supplied H_2O_2 was determined based on RRDE analysis.

^{1}H-NMR analysis of liquid products

The concentration of the liquid products was quantified by ^{1}H-NMR (Agilent 600 MHz). Typically, 430 μL sample was mixed with 50 μL of D_2O, and 20 μL of 6 mM dimethyl sulfoxide (DMSO, Sigma-Aldrich, 99.9%) was added as an internal standard.

^{13}C-NMR analysis of liquid products

Due to the lower detection limit of ^{13}C-NMR than that of ^{1}H-NMR, freeze-drying prior to analysis to combat low concentrations, frequently <100 μM C, was conducted[55]. 5 mL of 1 M KOH was mixed with 50 mL of sample to alkalify formic acid to formate anion to prevent sublimation during freeze-drying. Then sample was frozen by liquid nitrogen. Frozen sample was lyophilized at −80 °C at 200 mtorr until dry (48 h) (CH_3OH and CH_3OOH was sublimated in this step). Freeze-dried sample was re-dissolved in 1 mL DI water. 500 μL of re-dissolved sample was qualified by ^{13}C-NMR (Agilent 600 MHz).

GC analysis of gas products

The gas products from the EMPO reaction were quantified by on-line gas chromatography (GC, Agilent 6890). A flame ionization detector was used to detect CO and CO_2. A methanizer was utilized to increase the detection sensitivity of CO and CO_2. The GC system was equipped with a ShinCarbon ST column (Restek) to separate gas products. The calibration of the GC was carried out by flowing three calibration gas mixtures with CO- and CO_2-concentrations ranging from 10 to 100 ppm (Supplementary Fig. 25).

EPR experiment

The EPR spectrum of electrolytes was measured at KBSI Seoul Western Center using CW/Pulse EPR system with the following parameters: frequency 9.852 GHz; power 3 mW; modulation frequency 100 kHz; modulation amplitude 1 G; time constant 20.48 ms; conversion time 20.00 ms; scan 8; room temperature.

Synthesis of CH_3OOH

The CH_3OOH was synthesized by the modified procedures from the previously-reported method[56]. On the three-neck flask, 62.5 g of H_2O, 37.5 g of 30% H_2O_2, and 25 g of dimethyl sulfate ($(CH_3O)_2SO_2$, Sigma-Aldrich, ≥99.5%) were mixed. Subsequently, 52.5 g of 40 wt% KOH aqueous solution was added dropwise very slowly into the solution with stirring to induce a nucleophilic substitution reaction. The overall reaction is exothermic. Then, the gas-phase products were generated by the heat of the reaction. The generated gas-phase products were collected as a liquid phase in the vial by the condensation. Diluting the concentrated CH_3OOH in the DI water, electrochemical analysis was performed. The synthesized CH_3OOH was confirmed and quantified by ^{1}H-NMR analysis (Supplementary Fig. 26).

Reduction reaction test of CH_3OOH, CH_3OH, and HCOOH

The reducibility test of CH_3OOH, CH_3OH, and HCOOH (Sigma-Aldrich, ≥98%) were also performed in the similar electrochemical configurations as mentioned above. A working electrode prepared by spraying a-KB based catalyst ink on carbon paper (11.25 cm^2) was used. The mass loading of a-KB on the carbon paper was 1 mg cm^{-2}. Before the test, CV was carried out for the electrochemical cleaning of the electrode surface between 0.05 and 1.2 V (vs. RHE) at a scan rate of 100 mV s^{-1} for 20 cycles in N_2-saturated 0.05 M H_2SO_4. LSV was then performed from 1.1 to 0.1 V (vs. RHE) at a scan rate of 10 mV s^{-1} in N_2-saturated 0.05 M H_2SO_4 containing 0, 10, 20, and 40 mM of CH_3OOH, CH_3OH, and HCOOH, respectively.

Calculation of Gibbs free energy and standard potential

Standard Gibbs free energies of selected coupled reactions and their corresponding standard cell potentials have been calculated by Eqs. (8, 9) based on thermodynamic data (Supplementary Table. 3)[57]

$$\triangle G = \triangle H - T\triangle S \quad (8)$$

$$E = \frac{-\triangle G}{nF} \quad (9)$$

Data availability

The authors declare that the data supporting the findings of this study are available within the article and its Supplementary Information files. Source data are provided as a Source Data file. Additional data are available from the corresponding author upon reasonable request. Source data are provided with this paper.

References

1. Schwach, P., Pan, X. & Bao, X. Direct conversion of methane to value-added chemicals over heterogeneous catalysts: challenges and prospects. *Chem. Rev.* **117**, 8497–8520 (2017).
2. Ravi, M., Ranocchiari, M. & van Bokhoven, J. A. The direct catalytic oxidation of methane to methanol—a critical assessment. *Angew. Chem. Int. Ed.* **56**, 16464–16483 (2017).
3. Balcombe, P., Speirs, J. F., Brandon, N. P. & Hawkes, A. D. Methane emissions: choosing the right climate metric and time horizon. *Environ. Sci. Process. Impacts* **20**, 1323–1339 (2018).
4. Elvidge, C. D., Zhizhin, M., Baugh, K., Hsu, F.-C. & Ghosh, T. Methods for global survey of natural gas flaring from visible infrared imaging radiometer suite data. *Energies* **9**, 14 (2016).
5. Jin, Z. et al. Hydrophobic zeolite modification for in situ peroxide formation in methane oxidation to methanol. *Science* **367**, 193–197 (2020).
6. Xie, P. et al. Oxo dicopper anchored on carbon nitride for selective oxidation of methane. *Nat. Commun.* **13**, 1375 (2022).
7. Luo, L. et al. Binary Au–Cu reaction sites decorated ZnO for selective methane oxidation to C_1 oxygenates with nearly 100% selectivity at room temperature. *J. Am. Chem. Soc.* **144**, 740–750 (2022).
8. Meng, X. et al. Direct methane conversion under mild condition by thermo-, electro-, or photocatalysis. *Chem* **5**, 2296–2325 (2019).
9. Choudhary, T. V. & Choudhary, V. R. Energy-efficient syngas production through catalytic oxy-methane reforming reactions. *Angew. Chem. Int. Ed.* **47**, 1828–1847 (2008).
10. Sun, P. et al. Criteria air pollutants and greenhouse gas emissions from hydrogen production in U.S. steam methane reforming facilities. *Environ. Sci. Technol.* **53**, 7103–7113 (2019).
11. Buzcu-Guven, B. & Harriss, R. Extent, impacts and remedies of global gas flaring and venting. *Carbon Manag.* **3**, 95–108 (2012).
12. Periana, R. A. et al. A mercury-catalyzed, high-yield system for the oxidation of methane to methanol. *Science* **259**, 340–343 (1993).

13. Periana, R. A. et al. Platinum catalysts for the high-yield oxidation of methane to a methanol derivative. *Science* **280**, 560–564 (1998).
14. Jones, C. et al. Selective oxidation of methane to methanol catalyzed, with C-H activation, by homogeneous, cationic gold. *Angew. Chem. Int. Ed.* **43**, 4626–4629 (2004).
15. Starokon, E. V. et al. Oxidation of methane to methanol on the surface of FeZSM-5 zeolite. *J. Catal.* **300**, 47–54 (2013).
16. Groothaert, M. H., Smeets, P. J., Sels, B. F., Jacobs, P. A. & Schoonheydt, R. A. Selective oxidation of methane by the Bis(μ-oxo) dicopper core stabilized on ZSM-5 and mordenite zeolites. *J. Am. Chem. Soc.* **127**, 1394–1395 (2005).
17. Sushkevich, V. L., Palagin, D., Ranocchiari, M. & Bokhoven, J. A. Selective anaerobic oxidation of methane enables direct synthesis of methanol. *Science* **356**, 523–527 (2017).
18. Hammond, C. et al. Direct catalytic conversion of methane to methanol in an aqueous medium by using copper-promoted Fe-ZSM-5. *Angew. Chem. Int. Ed.* **51**, 5129–5133 (2012).
19. Cui, X. et al. Room-temperature methane conversion by graphene-confined single iron atoms. *Chem.* **4**, 1902–1910 (2018).
20. Bai, S. et al. High-efficiency direct methane conversion to oxygenates on a cerium dioxide nanowires supported rhodium single-atom catalyst. *Nat. Commun.* **11**, 954 (2020).
21. Wu, B. et al. Tandem catalysis for selective oxidation of methane to oxygenates using oxygen over PdCu/Zeolite. *Angew. Chem. Int. Ed.* **61**, e202204116 (2022).
22. Qi, G. et al. Au-ZSM-5 catalyses the selective oxidation of CH_4 to CH_3OH and CH_3COOH using O_2. *Nat. Catal.* **5**, 45–54 (2022).
23. Rocha, R. S., Camargo, L. M., Lanza, M. R. V. & Bertazzoli, R. A feasibility study of the electro-recycling of greenhouse gases: Design and characterization of a (TiO_2/RuO_2)/PTFE gas diffusion electrode for the electrosynthesis of methanol from methane. *Electrocatalysis* **1**, 224–229 (2010).
24. Rocha, R. S., Reis, R. M., Lanza, M. R. V. & Bertazzoli, R. Electrosynthesis of methanol from methane: the role of V_2O_5 in the reaction selectivity for methanol of a TiO_2/RuO_2/V_2O_5 gas diffusion electrode. *Electrochim. Acta* **87**, 606–610 (2013).
25. Boyd, M. J. et al. Electro-oxidation of methane on platinum under ambient conditions. *ACS Catal.* **9**, 7578–7587 (2019).
26. Song, Y. et al. Electrocatalytic oxidation of methane to ethanol via NiO/Ni interface. *Appl. Catal., B.* **270**, 118888 (2020).
27. Frese, K. W. Partial electrochemical oxidation of methane under mild conditions. *Langmuir* **7**, 13–15 (1991).
28. Tomita, A., Nakajima, J. & Hibino, T. Direct oxidation of methane to methanol at low temperature and pressure in an electrochemical fuel cell. *Angew. Chem. Int. Ed.* **47**, 1462–1464 (2008).
29. Lee, B., Sakamoto, Y., Hirabayashi, D., Suzuki, K. & Hibino, T. Direct oxidation of methane to methanol over proton conductor/metal mixed catalysts. *J. Catal.* **271**, 195–200 (2010).
30. Sa, Y. J., Kim, J. H. & Joo, S. H. Active edge-site-rich carbon nanocatalysts with enhanced electron transfer for efficient electrochemical hydrogen peroxide production. *Angew. Chem. Int. Ed.* **58**, 1100–1105 (2019).
31. Lu, Z. et al. High-efficiency oxygen reduction to hydrogen peroxide catalysed by oxidized carbon materials. *Nat. Catal.* **1**, 156–162 (2018).
32. Datsyuk, V. et al. Chemical oxidation of multiwalled carbon nanotubes. *Carbon* **46**, 833–840 (2008).
33. Zhang, H., Li, Y., Zhao, Y., Li, G. & Zhang, F. Carbon black oxidized by air calcination for enhanced H_2O_2 generation and effective organics degradation. *ACS Appl. Mater. Interfaces* **11**, 27846–27853 (2019).
34. Kundu, S., Wang, Y., Xia, W. & Muhler, M. Thermal stability and reducibility of oxygen-containing functional groups on multiwalled carbon nanotube surfaces: A quantitative high-resolution XPS and TPD/TPR study. *J. Phys. Chem. C* **112**, 16869–16878 (2008).
35. Huang, W. et al. Low-temperature transformation of methane to methanol on Pd_1O_4 single sites anchored on the internal surface of microporous silicate. *Angew. Chem. Int. Ed.* **55**, 13441–13445 (2016).
36. Hudson, R. et al. CO_2 reduction driven by a pH gradient. *Proc. Natl. Acad. Sci. USA* **117**, 22873–22879 (2020).
37. Xiao, F. et al. Selective electrocatalytic reduction of oxygen to hydroxyl radicals via 3-electron pathway with FeCo alloy encapsulated carbon aerogel for fast and complete removing pollutants. *Angew. Chem. Int. Ed.* **60**, 10375–10383 (2021).
38. Zhang, P. et al. Generation pathway of hydroxyl radical in Fe/N/C-based oxygen reduction electrocatalysts under acidic media. *J. Phys. Chem. Lett.* **12**, 7797–7803 (2021).
39. Buettner, G. R. Spin Trapping: ESR parameters of spin adducts 1474 1528V. *Free Radic. Biol. Med.* **3**, 259–303 (1987).
40. Buettner, G. R. The spin trapping of superoxide and hydroxyl free radicals with DMPO (5,5-Dimethylpyrroline-N-oxide): More about iron. *Free Radic. Res. Commun.* **19**, s79–s87 (1993).
41. Cuesta, A., Escudero, M., Lanova, B. & Baltruschat, H. Cyclic voltammetry, FTIRS, and DEMS study of the electrooxidation of carbon monoxide, formic acid, and methanol on cyanide-modified Pt(111) electrodes. *Langmuir* **25**, 6500–6507 (2009).
42. Rountree, E. S., McCarthy, B. D., Eisenhart, T. T. & Dempsey, J. L. Evaluation of homogeneous electrocatalysts by cyclic voltammetry. *Inorg. Chem.* **53**, 9983–10002 (2014).
43. Ab Rahim, M. H. et al. Oxidation of methane to methanol with hydrogen peroxide using supported gold–palladium alloy nanoparticles. *Angew. Chem. Int. Ed.* **52**, 1280–1284 (2013).
44. Yu, T. et al. Highly selective oxidation of methane into methanol over Cu-promoted monomeric Fe/ZSM-5. *ACS Catal.* **11**, 6684–6691 (2021).
45. Bauschlicher, C. W. & Partridge, H. The C-H dissociation energy of C_2H_6. *Chem. Phys. Lett.* **239**, 246–251 (1995).
46. Ruscic, B. Active thermochemical tables: Sequential bond dissociation enthalpies of methane, ethane, and methanol and the related thermochemistry. *J. Phys. Chem. A* **119**, 7810–7837 (2015).
47. Song, H. et al. Direct and selective photocatalytic oxidation of CH_4 to oxygenates with O_2 on cocatalysts/ZnO at room temperature in water. *J. Am. Chem. Soc.* **141**, 20507–20515 (2019).
48. Zhou, W. et al. Highly selective aerobic oxidation of methane to methanol over gold decorated zinc oxide via photocatalysis. *J. Mater. Chem. A* **8**, 13277–13284 (2020).
49. Song, H. et al. Selective photo-oxidation of methane to methanol with oxygen over dual-cocatalyst-modified titanium dioxide. *ACS Catal.* **10**, 14318–14326 (2020).
50. Fan, Y. et al. Selective photocatalytic oxidation of methane by quantum-sized bismuth vanadate. *Nat. Sustain.* **4**, 509–515 (2021).
51. Luo, L. et al. Water enables mild oxidation of methane to methanol on gold single-atom catalysts. *Nat. Commun.* **12**, 1218 (2021).
52. Sun, Z., Wang, C. & Hu, Y. H. Highly selective photocatalytic conversion of methane to liquid oxygenates over silicomolybdic-acid/TiO_2 under mild conditions. *J. Mater. Chem. A* **9**, 1713–1719 (2021).
53. Xu, Y. et al. Au decorated Pd nanowires for methane oxidation to liquid C_1 products. *Appl. Catal. B* **308**, 121223 (2022).
54. Luo, L. et al. Synergy of Pd atoms and oxygen vacancies on In_2O_3 for methane conversion under visible light. *Nat. Commun.* **13**, 2930 (2022).
55. Whitty, S. D., Waggoner, D. C., Cory, R. M., Kaplan, L. A. & Hatcher, P. G. Direct noninvasive ^{1}H NMR analysis of stream water DOM: Insights into the effects of lyophilization compared with whole water. *Magn. Reson. Chem.* **59**, 540–553 (2021).
56. Davies, D. M. & Deary M. E. A convenient preparation of aqueous methyl hydroperoxide and a comparison of its reactivity towards triacetylethylenediamine with that of other nucleophiles: The mechanism of peroxide bleach activation. *J. Chem. Soc., Perkin Trans. 2*, 559–562 (1992).

57. Goldsmith, C. F., Magoon, G. R. & Green, W. H. Database of small molecule thermochemistry for combustion. *J. Phys. Chem. A* **116**, 9033–9057 (2012).

Acknowledgements

This work was supported by Yonsei-KIST Convergence Research Program (J.H.P) and Yonsei Fellow Program, funded by Lee Youn Jae (J. K.). The National Research Foundation of Korea (NRF) grant funded by the Korea government (NRF–2021R1A5A1084921 and 2021M3H4A1A03057403 (Y.J.H.), NRF-2019R1A2C3010479 (J.H.P.)), the Institute for Basic Science (IBS-R006-D1; Y.J.H.), and Creative-Pioneering Researchers Program through Seoul National University also support this work (Y.J.H.).

Author contributions

Y.J.H. and J.H.P. conceived and supervised the project. J.K., J.H.K., J.H.P., and Y.J.H. prepared the manuscript. J.H.K. and J.K. synthesized the electrocatalyst and performed electrochemical experiments. J.H.K. synthesized CH_3OOH and E.L. assisted synthesis process. J.K. and H.Y. conducted characterization of the electrocatalyst. J.K. and C.O. performed NMR analysis. C.O., H.O., J.H.P., and Y.J.H. provided advice and expertise. All authors discussed the result and commented on the manuscripts.

Competing interests

The authors declare no competing interests.

Additional information

Supplementary information The online version contains supplementary material available at https://doi.org/10.1038/s41467-023-40415-6.

Correspondence and requests for materials should be addressed to Jong Hyeok Park or Yun Jeong Hwang.

Peer review information *Nature Communications* thanks Nikolay Kornienko and the other, anonymous, reviewer(s) for their contribution to the peer review of this work. A peer review file is available.

Reprints and permissions information is available at http://www.nature.com/reprints

Publisher's note Springer Nature remains neutral with regard to jurisdictional claims in published maps and institutional affiliations.

Open Access This article is licensed under a Creative Commons Attribution 4.0 International License, which permits use, sharing, adaptation, distribution and reproduction in any medium or format, as long as you give appropriate credit to the original author(s) and the source, provide a link to the Creative Commons licence, and indicate if changes were made. The images or other third party material in this article are included in the article's Creative Commons licence, unless indicated otherwise in a credit line to the material. If material is not included in the article's Creative Commons licence and your intended use is not permitted by statutory regulation or exceeds the permitted use, you will need to obtain permission directly from the copyright holder. To view a copy of this licence, visit http://creativecommons.org/licenses/by/4.0/.

© The Author(s) 2023